**Annals Geol. Surv. Egypt. V.XXXIX (2022), pp. 109 - 143**

# EVALUATION OF LATE MIOCENE HYDROCARBON RESERVOIRS, THROUGH COMPUTER PROCESSED INTERPRETATIONS ON THE WELL LOG DATA OF NIDOCO FIELD, NILE DELTA, EGYPT

**BY**

El-Kadi, H. H. [(1)], Ali, M. F. M. [(1)] and Omar, Mustafa [(2)]
[(1)] AL-Azhar University, [(2)] Belayim Petroleum Company, Cairo, Egypt.

**ABSTRACT**

*The present study deals with a comprehensive interpretation of the available well-log data at the Central part of the Nile Delta (Nidoco Field). The regional geologic setting of the area was discussed before going deeply in the petrophysical interpretation of the study area. The geologic interpretation was started by good geologic correlation, subdividing the studied Late Miocene section into levels and units. These levels and units are correlated among wells, according to their remarkable changes in log responses and similarity.*

*Tri-porosity (M-N) cross-plots for mineral identifications were used, to detect in general the types of lithology. Lithological identification is achieved through the cross-plots between ρb, Øn and Δt to detect the exact lithology for each layer. These plots showed that, sandstone and shale represent the main components of the Late Miocene section. Pickett's plots were constructed to determine the formation water resistivity (Rw), and the water and hydrocarbon saturations (Sw and Shr). Dia-porosity cross-plots were established, to determine the shale volume (Vsh) and effective porosity (Øeff). Shale types cross-plots were used also to detect the shale types in the studied section, which are mainly laminated with a mixture of dispersed shales. Shale minerals cross-plots were used too to indicate that, Montmorillonite is the main shale component in the studied section.*

*The petrophysical characteristics of the studied wells were represented vertically in the form of litho-saturation cross-plots inferred from the computer processed interpretation (CPI). The lateral variations of the mentioned petrophysical characteristics were represented in the form of iso-parametric maps (shale content, effective porosity and hydrocarbon saturation).*

*The petrophysical characteristics of studied levels and units reflect the ability of some layers to store and produce hydrocarbon. It is clear that, Level-2, Level-3, Level-3A, Level-3 Lower, Unit-A and Unit-B show better reservoir characterization and higher gas potentialities than these of the remaining studied levels and units. According to these results, it is recommended to drill more exploratory and development wells, to produce more hydrocarbons from the study area, which is thought to preserve high hydrocarbon potentialities.*

## INTRODUCTION

In the last three decades, gas has become a very important source of energy in the world, due to its low cost and environmental impact. The demands for gas energy were remarkably increasing, especially with the spread of frequent environmental hazards caused by the extensive use of the classical energy sources. In Egypt, the Nile Delta region has been considered as one of the most important gas provinces, as its sedimentary succession seems to hide high gas potentialities. The first exploration license in the Nile Delta region, issued to the International Egyptian Oil Company (IEOC), a subsidiary of Ente Nazionale Idrocarburi (Eni) in 1963. The first onshore well, Mit Ghamr-1, drilled by IEOC in

1966. The first discovery made by IEOC in 1967, with the drilling of Abu Madi-1 well. Production of gas and condensate from Abu Madi field began in 1975. The studied area, Nidoco field is located in the offshore Nile Delta of Egypt, in Abu Madi West Development Lease operated by Petrobel, on the behalf of the concession shareholders EGPC 50%, IEOC 37.5%, and BP 12.5%. Nidoco field was discovered in 1993 by hitting Abu Madi Formation, Level-3 Main, as the main producing reservoir through Nidoco-6 well. In December 2012, the production was stopped, due to the high water production. So, additional work has started to find new opportunities. According to the results of work, new successful wells have been drilled, with huge added reserves in 2015.

**1. Location of the Study Area:**

The Nile Delta concession extends onshore and offshore, through the northern part of Egypt, between latitudes 30° 45' N and 32°30' N, and longitudes 29° 30' E and 33° 00' E. Nidoco gas and condensate field is located at the central part of Abu Madi Paleovalley area, which is bounded by El-Qara Field to the South and by Baltim South Field to the North.

Abu Madi West Development Lease was defined around the Nidoco field. The development lease is about 10 km off the Egyptian Coast, where the water depth of the Mediterranean Sea reaches 20 m (Figure 1).

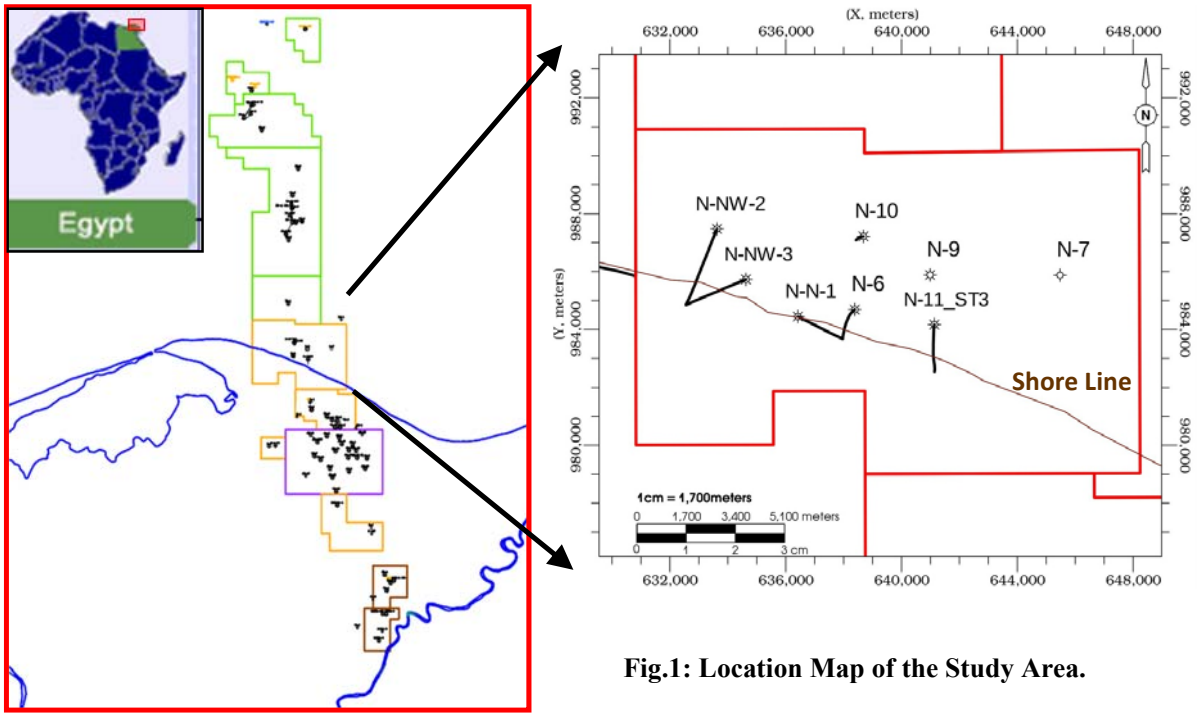


**Fig.1: Location Map of the Study Area.**

**2. Aim of the Present Study:**

The main objectives of this work are to interpret the well logs and to complete the petrophysical evaluation for the studied wells. In addition, based on the vertical and lateral variations of the petrophysical characteristics, the evaluation of hydrocarbon reservoirs of the Late Miocene section had been performed. This evaluation achieved through cross-plots and computer processed interpretation (CPI), by the application of sophisticated computer software, to determine the petrophysical characteristics in the area under investigation. These characteristics include; shale content, effective porosity, and water and hydrocarbon saturations by using the Density, Resistivity, Neutron porosity, Sonic, Nuclear Magnetic Resonance and Gamma-ray logs. The computer programs have been applied to the studied rock units of the Late Miocene section, which penetrated by eight wells distributed in the study area.

**3. Nile Delta Regional Geologic Setting:**

The geology of the Nile Delta was studied by many authors. In the following paragraphs, the brief review of the structures and stratigraphy of the Nile Delta is given.

Nile Delta Basin comprehends the continental shelf and slope, from 80 Km west of Alexandria to North Sinai, and the Nile submarine fan (Figure 2). The Nile submarine fan is a huge turbiditic complex, which can be divided into Rosetta Nile Cone and Damietta fans. In particular, the central and southern third of the Damietta fan is termed the Levant Platform .

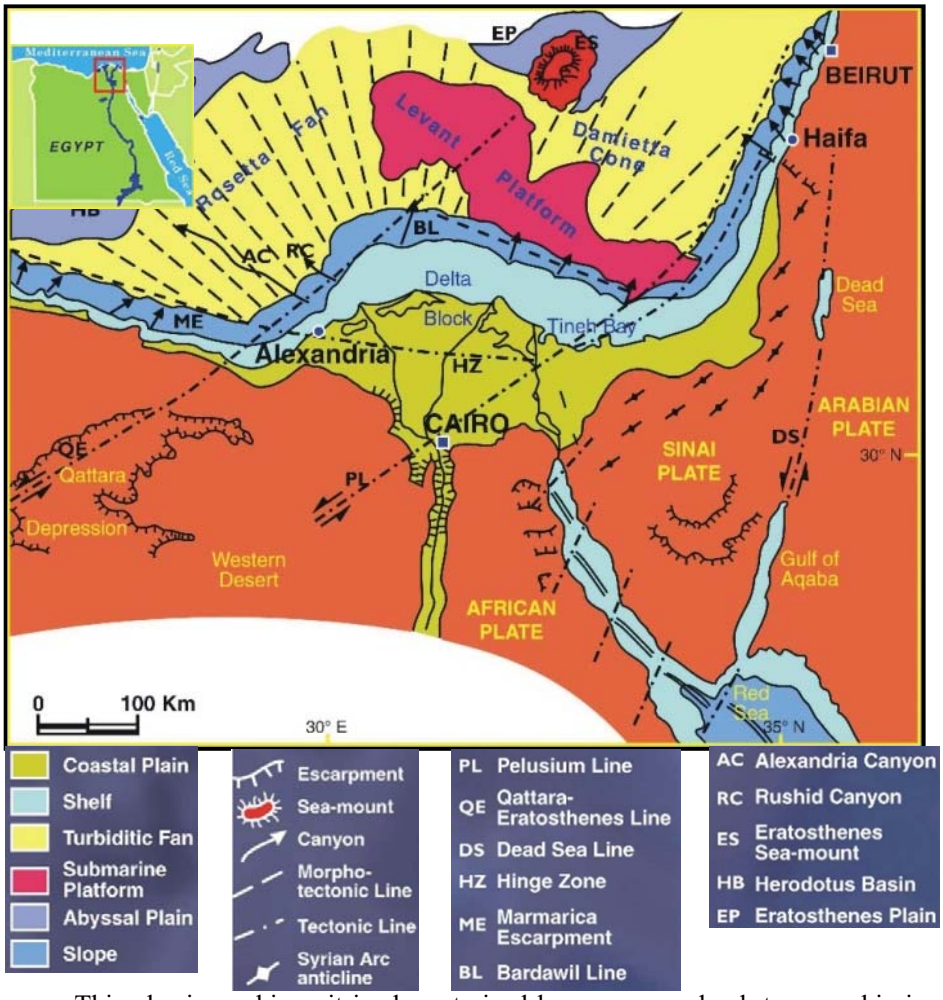


**Fig.2: Main Features of the Nile Delta and Eastern Mediterranean (Eni/Agip Internal Study, 2000).**

This physiographic unit is characterized by pronounced sub-topographic irregularities, mostly due to the vertical and horizontal flows of the Messinian evaporites and collapse of the crests of some diapirs. The two physiographic and tectonically controlled elements, which are located in correspondence of the northern slope off the Nile Delta and off the Western Desert, are termed Bardawil (or Misfaq) and Marmarica Escarpments, respectively. The two mainly NW-SE trending features are offset by the NE-SW Qattara-Eratosthenes and Pelusium trans-current faults, which in their offshore portions roughly coincide with the northwestern slope off Alexandria and the external limit of the continental margin off Palestine.

(Figure 3) represents the summary of the Tertiary generalized stratigraphic column, with the major tectonic events. Before going in details, stratigraphic units of the study area are introduced in (Table 1).

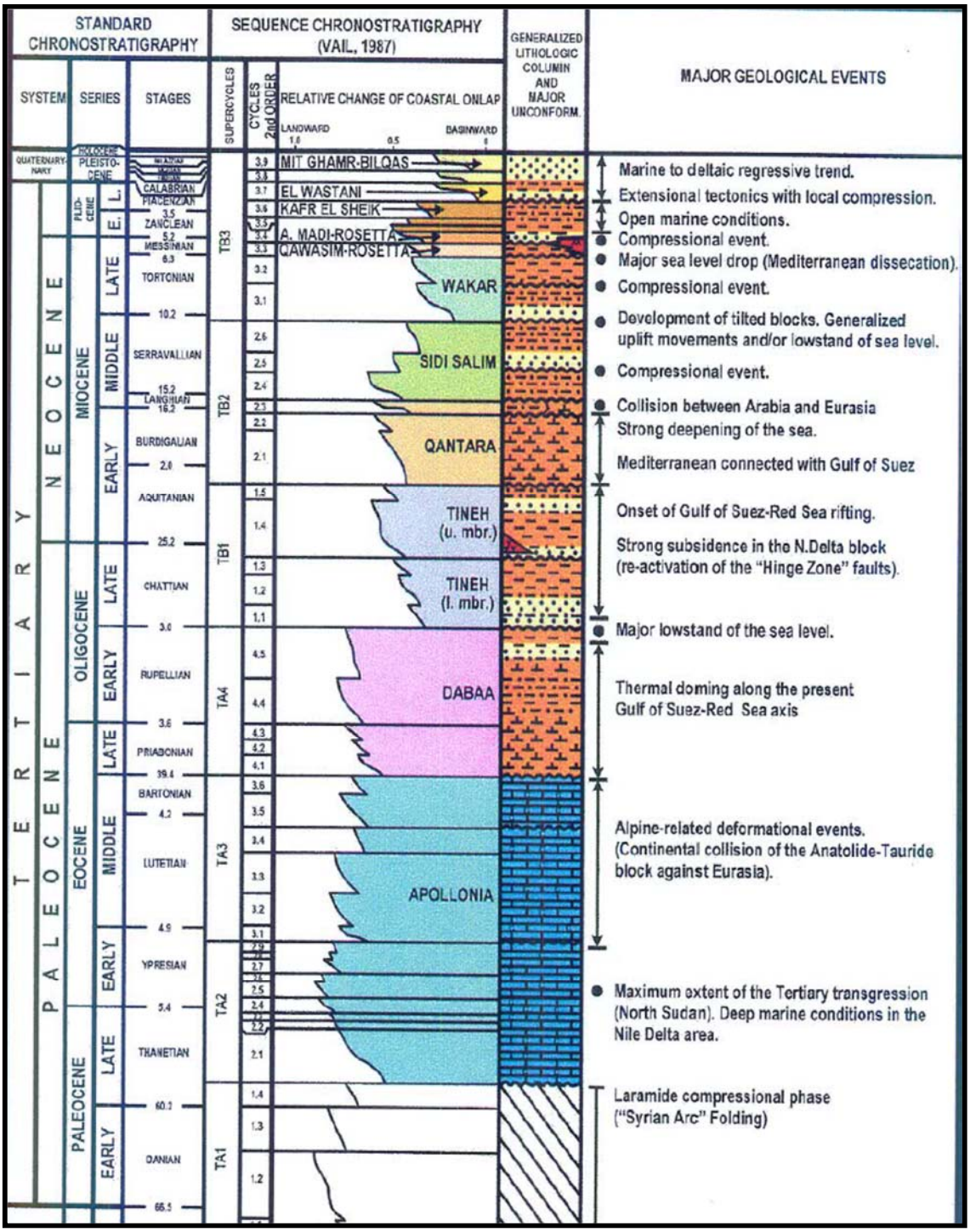


**Fig.3: Tertiary Generalized Stratigraphic Column with Major Tectonic Events (Eni/Agip Internal Study, 2000).**

**Table (1): The Stratigraphic Units of the Study Area.**

| Epoch | Age | Formation | Sub-Levels | Lithology |
|---|---|---|---|---|
| Pliocene | Zanclean | Kafr El Sheikh | --- | Shale |
| | | | Level-1 | Siltstone and Sandstone |
| Late Miocene | Messinian | Abu Madi | Messinian Sh | Shale |
| | | | Level-2 | Sandstone and Siltstone |
| | | | Level-2 Base | Shale |
| | | | Level-2A | Siltstone |
| | | | Level-2A Base | Shale |
| | | | Level-3A | Sandstone and Siltstone |
| | | | Level-3A Base | Shale |
| | | | Level-3 | Sandstone |
| | | | Level-3 Base | Shale |
| | | | Level-3 Lower | Sandstone |
| | | | Level-3 Lower Base | Shale |
| | | | Bottom Abu Madi | Unconformity |
| | | Qawasim | Unit-A | Sandstone and Siltstone |
| | | | Bottom Unit-A | Shale |
| | | | Unit-A1 | Sandstone and Siltstone |
| | | | Unit-B | Sandstone and Siltstone |
| | | | Bottom Unit-B | Shale |
| | | | Unit-C | Siltstone |
| | | | Bottom Unit-C | Shale |
| | | | Unit-D | Sandstone and Limestone |
| Middle Miocene | Serravallian | Sidi Salem | Serravallian | Shale |

## WELL-LOG ANALYSIS

Well-log analysis represents the most important stage in the evaluation of petrophysical characteristics, which involve shale content, effective porosity, and water and hydrocarbon saturations. In this study, two processes were applied to evaluate the petrophysical characteristics of the Miocene studied section. The first one is the cross plots evaluation, which depends on using the charts, while the second process is the application of the computer softwares (computer processed interpretation). Evaluation methods have evolved rapidly in recent years, as the results of more numerous and efficient tools, as well as the calculating capacity of computer, which is used nowadays during well operations. Highly efficient computer software provides complete and accurate evaluation. Interactive Petrophysics software (IP) is used in this study.

**1. Panels and Cross Plots Evaluation:**

Panels, diagrams and cross plots for the determination of petrophysical parameters were obtained graphically, to evaluate the Late Miocene section, by the exploration of its reservoir possibility and petroleum accumulation. In this study, the petrophysical evaluation process passes through qualitative and quantitative interpretation techniques. Quantitative techniques are based on a series of empirical relationships and models, or cross plots derived from simultaneous equations (Burke et al. 1969). One E-W correlation profile (Figure 4) is established, by using the information obtained from the available logs, especially the gamma ray, resistivity, sonic, density and Neutron. The used logs are divided into zones, to be correlated easily with each other in the eight wells, within the area under investigation.

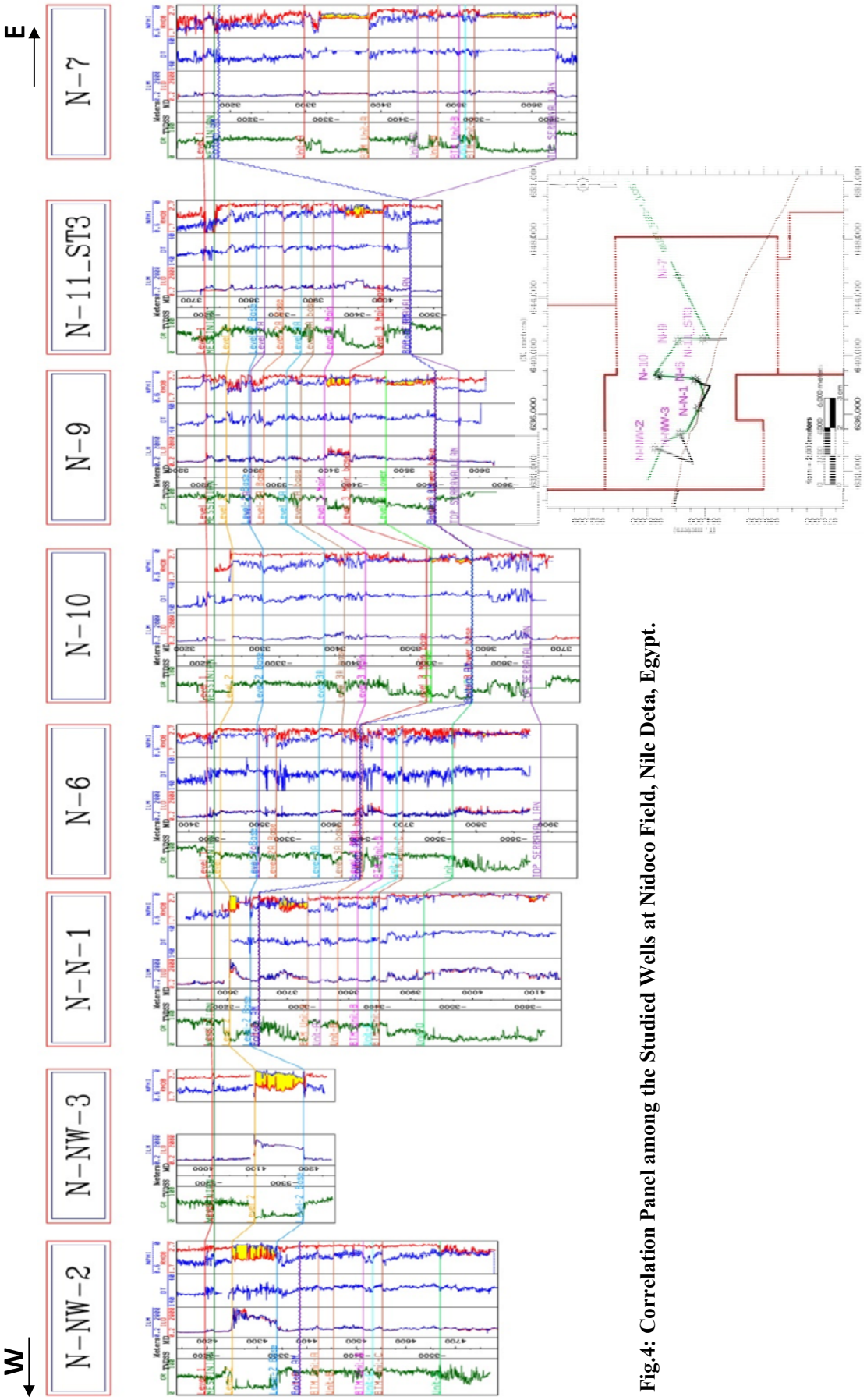


**Fig.4: Correlation Panel among the Studied Wells at Nidoco Field, Nile Deta, Egypt.**

**1.1. Qualitative Correlation:**

It is the process of comparing one log with another of the same type or different types that enables the interpreter to obtain more information than can be derived from only one log. The responses of Gamma Ray, Sonic, Density and Neutron curves to the various subsurface formations are found to be highly consistent over large area. Certain formations are easily recognizable from the unique shape of the response and provide an accurate indication of the strata (Mody, 1961).

**1.2. Quantitative Analysis:**

Quantitative log analysis is based on a series of empirical relationships or model equations. In this study, the applied quantitative techniques are using the charts and cross plots, which in fact are based on mathematical calculations by using the simultaneous equations.

**1. 2.1 M-N (Tri- Porosity) Cross-Plot:**

This technique depends on the fluid and log parameters, which are incorporated together essentially in the three porosity logs; Sonic, Density and Neutron. In complex lithologies, the M-N Cross Plots or Tri-porosity Cross Plots are used to identify the mineral mixtures. From the values of these porosity logs, two functions (M and N) are calculated, which are independent of the primary porosity; therefore a cross-plot of these two quantities gives generally the lithologic classification (Pirson, 1977). By using the M-N Plot for minerals identification, the lithologic content for each zone can be defined, with respect to the standard M-N values of the common minerals and rocks (Schlumberger, 1972).

(Figure 5) represents the M-N plot for twenty one layers (ten shaley and eleven non shaley) in seven wells. One of the studied eight wells, which is N-NW-3, did not record the sonic data, so there is no M-N cross plot for this well. The M-N cross-plot shows wide range of minerals, mainly shale, sandstone, gas sandstone, calcareous sandstone, limestone and dolomite.

**1.2.2. Lithologic Identification:**

Logs can be used as indicators of lithology. The most useful logs for this purpose are the Density, Neutron and Sonic. An important technique, giving an accurate result for the lithologic identification, is the use of cross-plots (Schlumberger charts) between $Ø_{CNL}$ Vs $\rho_b$, $Ø_{CNL}$ Vs $\Delta t$ and $\Delta t$ Vs $\rho_b$ log-readings, to obtain the lithologic characteristics and porosities. (Figure 6) represents $Ø_{CNL}$ Vs $\rho_b$ cross-plot of the Late Miocene studied section. The plotted values of the studied wells show that, the major and predominant lithology is the sandstone and shale layers, with few layers of limestone and dolomite. The gas effect also is clear on the chart in the gas-bearing zones. (Figure 7) represents $Ø_{CNL}$ Vs $\Delta t$ cross-plot of the Late Miocene studied section. The plotted values of the studied wells show that, the major and predominant lithology is the sandstone and shale layers with few layers of limestone. (Figure 8) represents $\Delta t$ Vs $\rho_b$ cross-plot of the Late Miocene studied section. The plotted values of the studied wells show that, the major and predominant lithology is the sandstone and shale layers. Sandstone porosity is ranging from 15 to 25 p.u., with some exceptions in the mixed lithology layers. It is clear also that, $Ø_{CNL}$ Vs $\rho_b$ cross-plot is more helpful than the last two ones.

**1.2.3. Pickett's Plots:**

Pickett's cross-plot (Deep Resistivity / Porosity) is a convenient way to demonstrate how various log combinations are responded to fluid and porosity. It is a double logarithmic plot of the resistivity measurements on the x-axis versus the porosity measurements on the y-axis. The plot is based on taking the logarithm of Archie's equation. Points of constant water saturation (Sw) will plot on a straight line, with negative slope of the value m. Water zones define the lowermost line on the plot. Since Sw = 1, the water resistivity can be determined from a point on the line. Once the water line is established, the other parallel lines can be drawn for the different water saturations, assuming a constant (n) (usually 2). In this study, the water resistivity (Rw) and water saturation (Sw) for the different horizons are determined by Pickett's cross plots. In addition, the collected formation water samples from the studied wells helped in detecting the water resistivity and water salinities. Fourteen Pickett's cross-plots for fourteen water-bearing zones were carried out, to detect the estimated water resistivity and salinities.

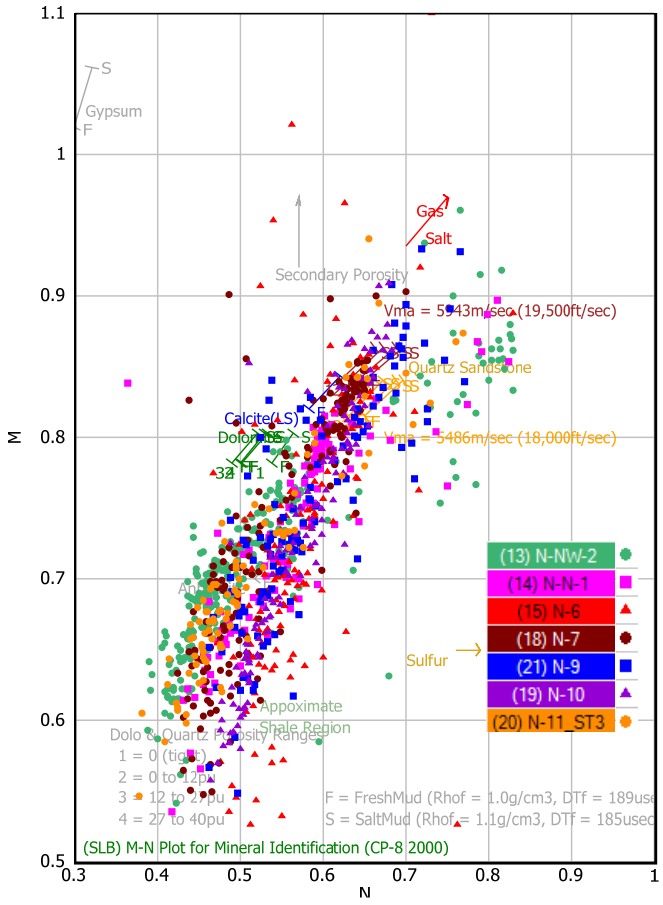


**Fig.5: M-N Plot for Mineral Identification for Studied wells.**

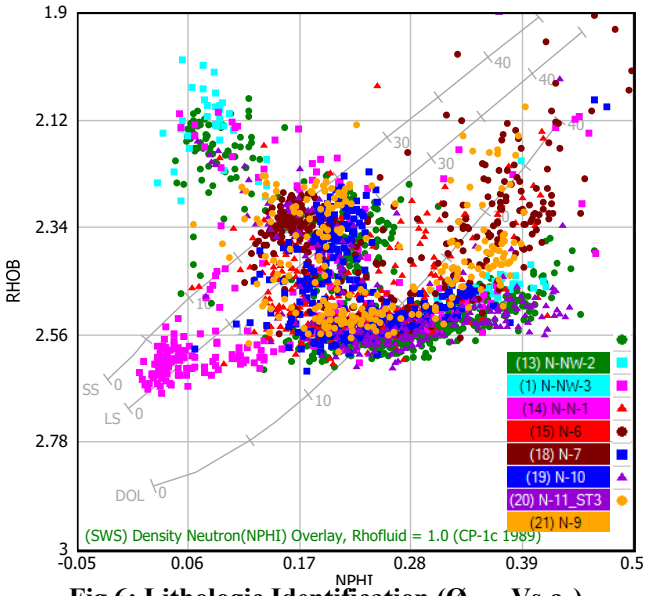


**Fig.6: Lithologic Identification ($Ø_{CNL}$ Vs $\rho_b$) Cross-Plot for Studied wells.**

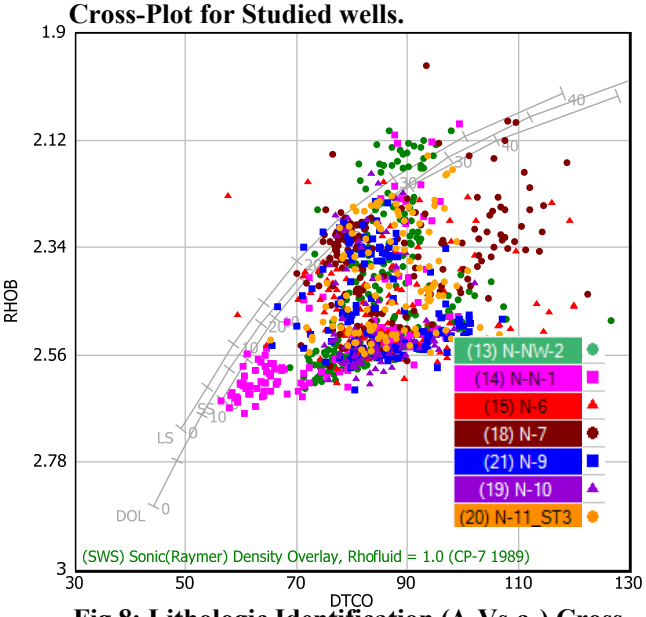


**Fig.8: Lithologic Identification ($\Delta_t$ Vs $\rho_b$) Cross-Plot. for Studied wells.**

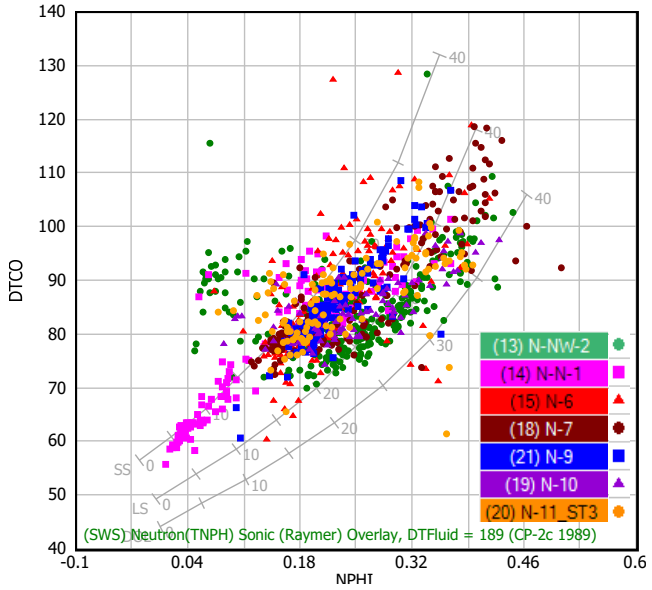


**Fig.7: Lithologic Identification ($Ø_{CNL}$ Vs $\Delta_t$) Cross-Plot for Studied wells.**

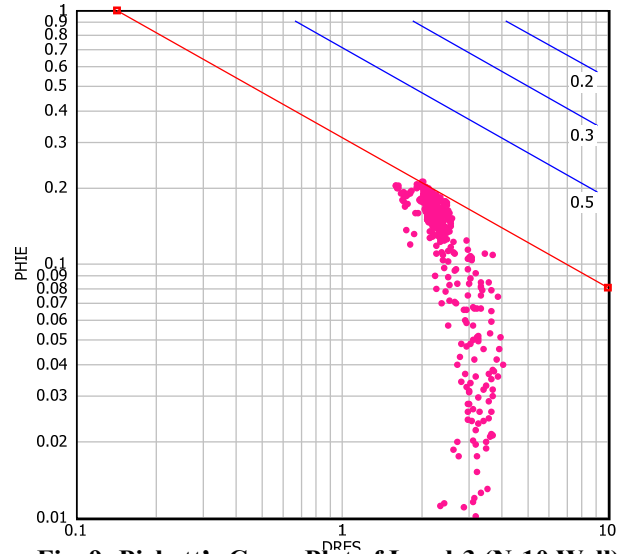


**Fig. 9: Pickett's Cross-Plot of Level-3 (N-10 Well).**

Also, four actual formation water samples from the studied wells were collected and analyzed, to detect the water resistivities (Rw) and salinities. The obtained formation water resistivities (Rw) range was from 0.138 Ohm.m to 0.20 Ohm.m, and the obtained hydrocarbon saturations (Shr) range was from 83% to 0%. (Figures 9-15)

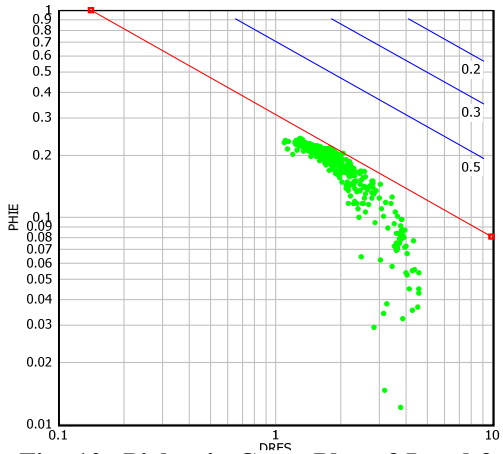


**Fig. 10: Pickett's Cross-Plot of Level-3 Lower for N-10 Well.**

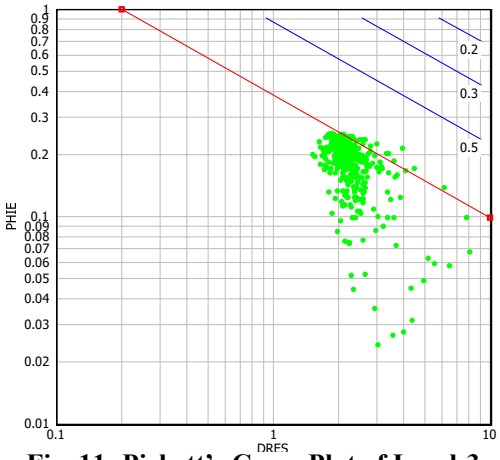


**Fig. 11: Pickett's Cross-Plot of Level-3 Lower for N-9 Well.**

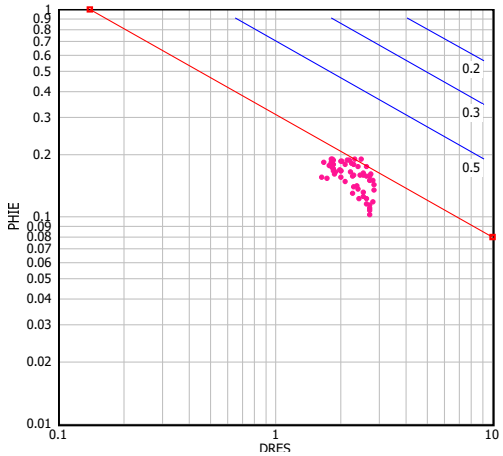


**Fig. 12: Pickett's Cross-Plot of Level-3 for N-11_ST3 Well.**

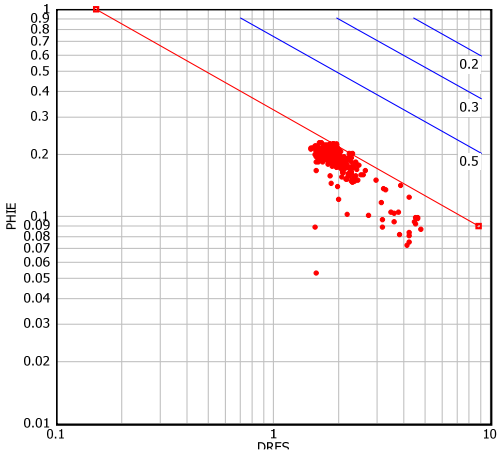


**Fig. 13: Pickett's Cross-Plot of Unit-A for N-7 Well.**

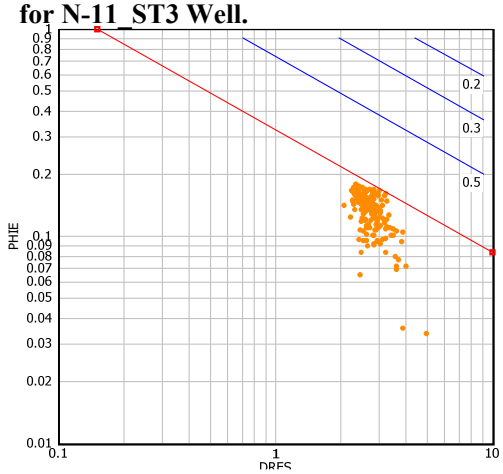


**Fig. 14: Pickett's Cross-Plot of Unit-B for N-7 Well.**

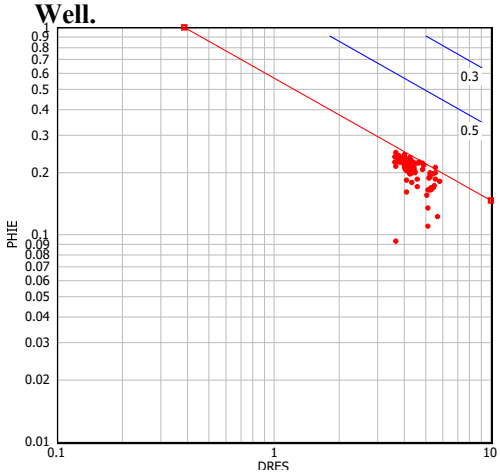


**Fig. 15: Pickett's Cross-Plot of Unit-A for N-N-1 Well.**

### 1.2.4. Dia-Porosity Cross-Plots:

For the determination of the effective porosity ($Ø_{eff}$) and shale volume ($_{Vsh}$), combinations of the porosity logs can be used. Three plots are used ($\rho_b$ Vs $Ø_{CNL}$, $\Delta t$ Vs $\rho b$ and $\Delta t$ Vs $Ø_{CNL}$) for each lithologic unit, within the studied section. The effective porosity and shale content for each zone are estimated, by calculating the mean value of the obtained $Ø_{eff}$ and $V_{sh}$. The triangle, which consists the cross-plot, is defined by the matrix point, water point and shale point. The matrix-water line and matrix-shale lines are linearly divided into effective porosities ($Ø_{eff}$) and shale volumes ($V_{sh}$) percentages, respectively. Some permeable horizons are shifted outside the triangle. The obtained shale volumes ($V_{sh}$) range was from 3% to 45% and the obtained effective porosities ($Ø_{eff}$) range was from 8% to 20 %. (Figs. 16- 18) are representing the Dia-porosity cross-plots for Level-2 layers, as an example, while the rest of the layers plots results were added directly to the final computer processed interpretation (CPI).

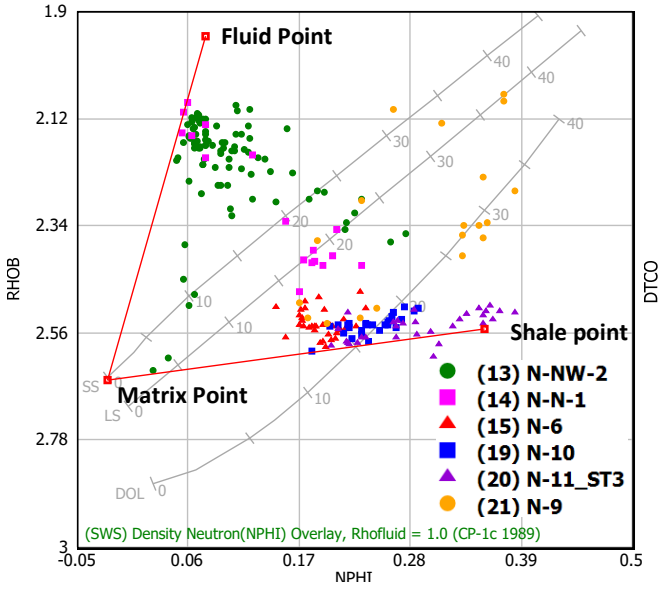


**Fig.16: Dia-Porosity ($\rho_b$ Vs $Ø_n$) Cross-Plot of Level-2.**

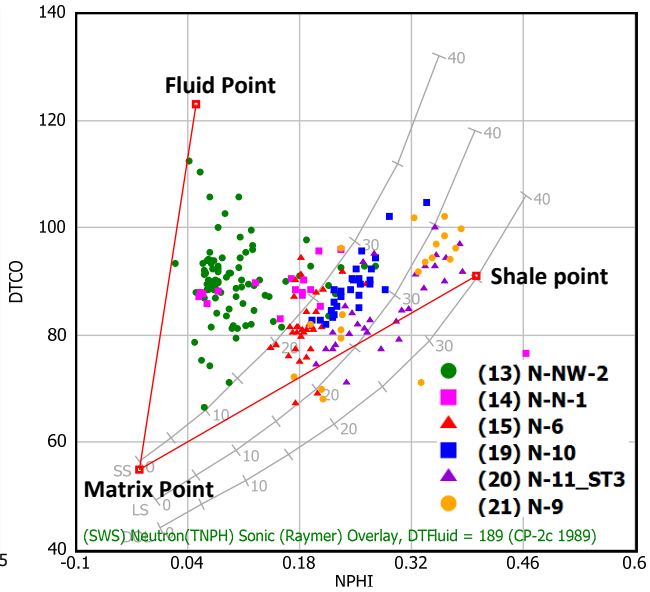


**Fig.17: Dia-Porosity ($\Delta t_{log}$ Vs $Ø_n$) Cross-Plot of Level-2.**

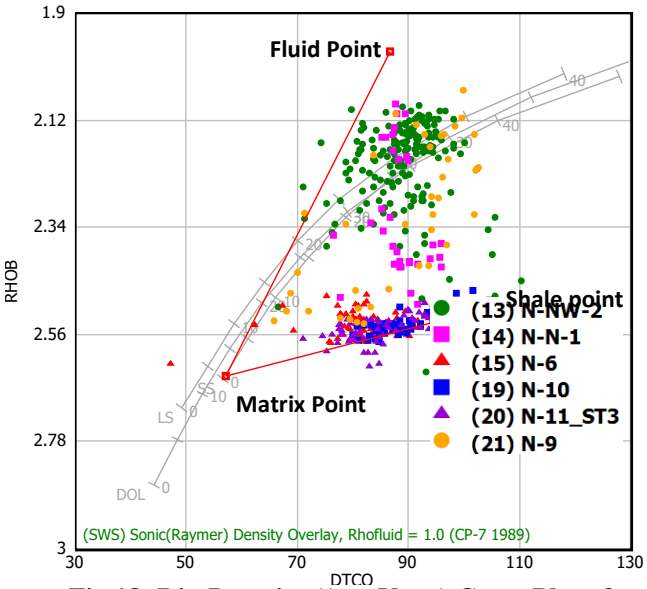


**Fig.18: Dia-Porosity ($\Delta t_{log}$ Vs $\rho_b$) Cross-Plot of Level-2.**

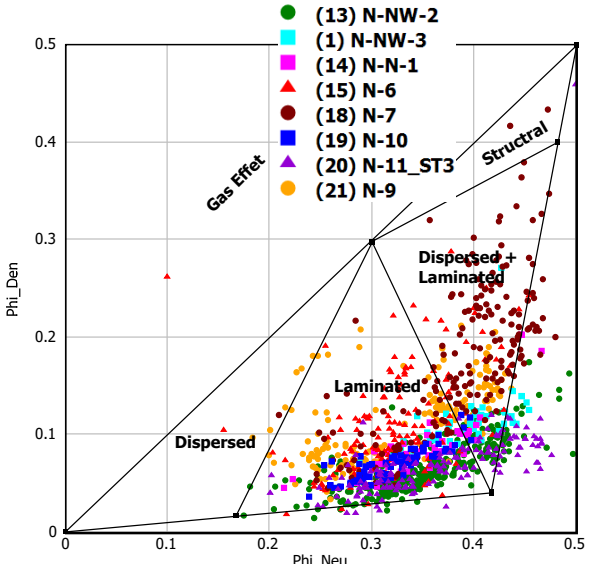


**Fig. 19: Shale Types ($Ø_n$ Vs $Ø_d$) Cross-Plot of All Shale Layers (after Darwin, 1987).**

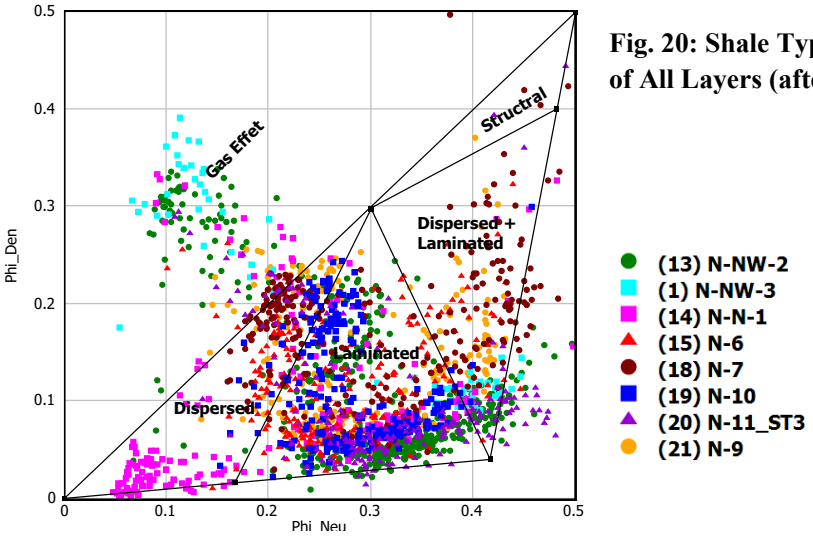


**Fig. 20: Shale Types ($Ø_n$ Vs $Ø_d$) Cross-Plot of All Layers (after Darwin, 1987).**

### 1.3. Shale Types:

Shaly materials can be distributed in the formation in three ways; laminated, structural and dispersed in the shaly sand (Darwin, 1987). (Figure 19) represents the shale model, which exhibits the cross-plot of $Ø_n$ Vs $Ø_d$, to determine the shale types present in the studied shale layers of the area under investigation. From this figure, it is clear that, the shale types in the studied formation are mostly laminated, with a mixture of laminated and dispersed shales. (Figure 20) represents another cross-plot, including the same shale layers of (Figure 19), plus all the sand and carbonate layers to show the shale types within these layers. It is obvious in this figure that, some reservoir layers are gas-bearing, which has an impact of the readings and shifting the points toward the lift and up directions.

### 1.4. Shale Minerals:

Three types of plots for shale minerals have been used in this study, using mainly the Natural Gamma-Ray Spectrometry (NGS) data, which recorded only in five studied wells. Four wells only have been used here, because the fifth one had very poor quality data (N-11_ST3 well).

#### 1.4.1. Thorium- Potassium Cross Plot:

This chart is used to determine the type of minerals in a shale formation, from the concentrations measured by the Natural Gamma-Ray Spectrometry tool (NGS). (Figure 21) represents the Thorium in PPM versus Potassium concentration in % cross plot, to determine the shale minerals present in the studied formations of the area under investigation. From this figure, it is clear that, the shale minerals in the studied shale layers is Montmorillonite.

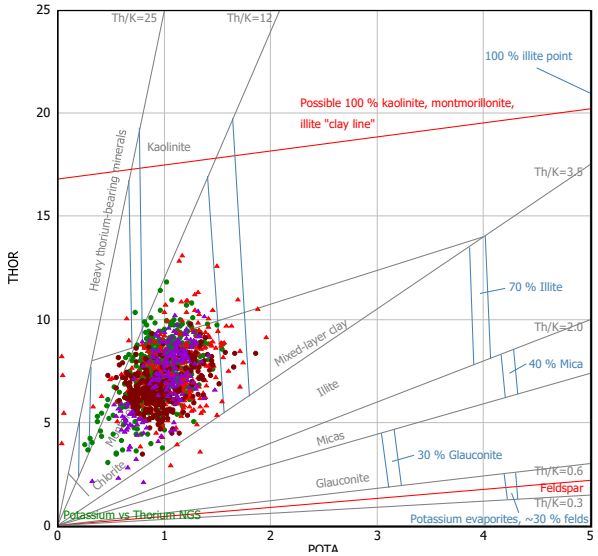


**Fig. 21: Shale Minerals (Th Vs K) Cross-Plot of All Shale Layers.**

### 1.4.2. Photoelectric Factor- Potassium Cross Plot:

This chart is a method for identifying the type of clay minerals in the wellbore. The values of the photoelectric factor (PEF) from the Litho-Density log and the concentration of potassium (K) from the Natural Gamma-Ray Spectrometry (NGS) tool are plotted on the chart. (Figure 22) represents the Photoelectric Factor in B/E versus potassium concentration in % cross plot, to determine the shale minerals present in the studied formations of the area under investigation. Observe here in most of the wells that, all the PEF readings are affected by the mud (the readings are higher than usual, because of the mud additives). So, the PEF readings can be shifted down on the plot, to make good estimation of the shale minerals. If the shift is applied, it is likely that, the shale minerals in the studied shale layers is Montmorillonite.

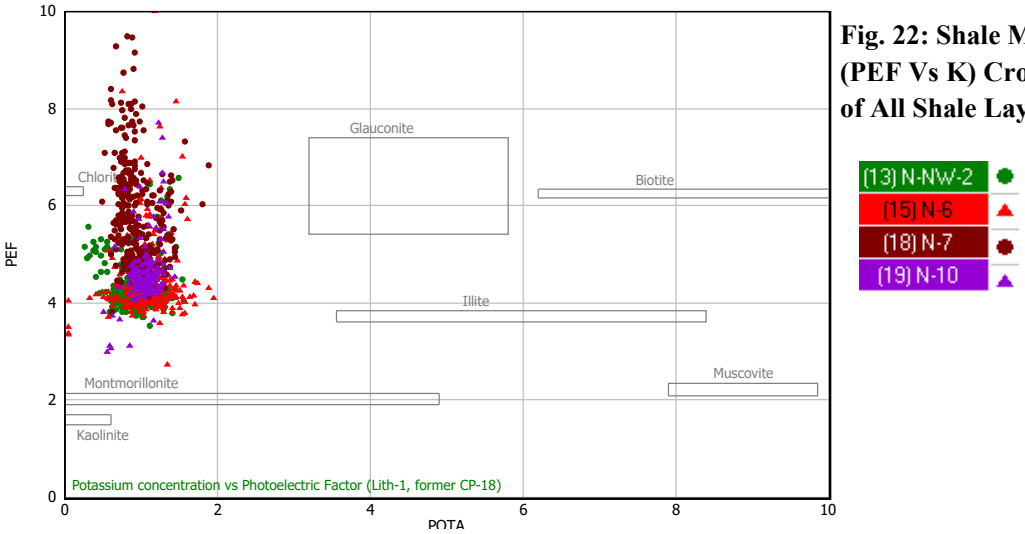


**Fig. 22: Shale Minerals (PEF Vs K) Cross-Plot of All Shale Layers.**

### 1.4.3. Photoelectric Factor- Thorium/Potassium Ratio Cross Plot:

This chart is a method for identifying the type of clay minerals in the wellbore. The values of the photoelectric factor (PEF) from the Litho-Density log and the ratio of thorium and potassium (Th/K) from the Natural Gamma-Ray Spectrometry (NGS) tool are plotted on the chart. (Figure 23) represents the Photoelectric Factor in B/E versus thorium per potassium concentration in ratio cross plot, to determine the shale minerals present in the studied formations of the area under investigation. Observe here in most of the wells that, all the PEF readings are affected by the mud (the readings are higher than usual, because of the mud additives). So, the PEF readings can be shifted down on the plot too, to make good estimation of the shale minerals. If the shift is applied, it is likely that, the shale minerals in the studied shale layers is Montmorillonite.

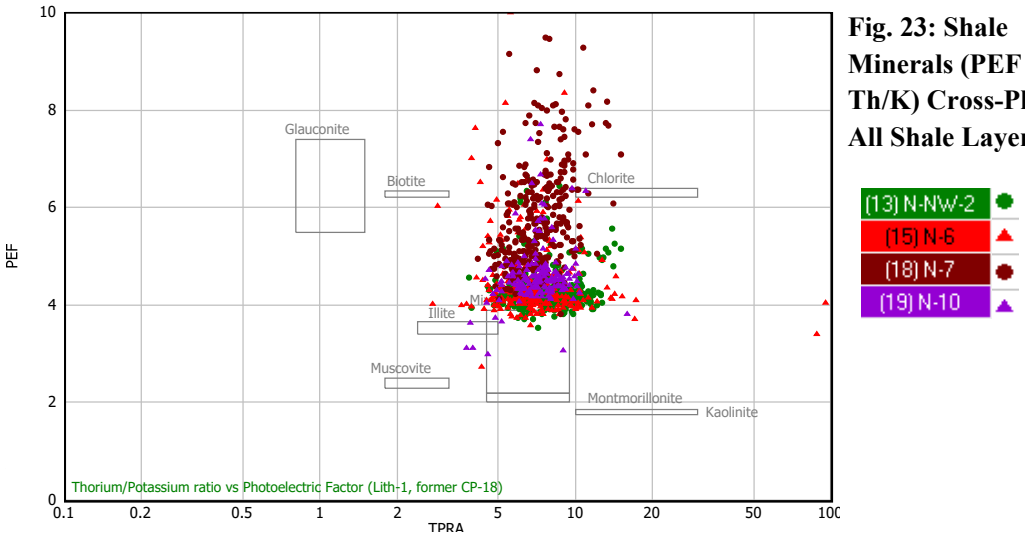


**Fig. 23: Shale Minerals (PEF Vs Th/K) Cross-Plot of All Shale Layers.**

One of the features of modern log interpretation is the systematic usage of computer softwares. This makes possible to rapid integration of several logging measurements, acquired separately, with all other available bore holes and geologic information. As a result, the detection and evaluation of potential hydrocarbon-bearing zones can nowadays be generally achieved at the well-site, right after the logging operation (quick-look).

In this study, Interactive Petrophysics software (IP) is developed by Senergy, which has more or less inspired all other similar softwares, is used to evaluate the petrophysical characteristics of the studied formations in the form of litho-saturation plots. This Interactive Petrophysics computer program was designed for the quantitative formation evaluation of the open and cased-hole logs. (Figs. 24-26) represent the computer processed interpretation (CPI) correlations obtained from Interactive Petrophysics software for the studied wells.

## LLUSTRATION OF RESULTS

In this study, the hydrocarbon potentialities of the Late Miocene section have been evaluated by studying the petrophysical characteristics of the different horizons.

### 1. Lateral Variations of Petrophysical Characteristics:

The lateral variation of petrophysical characteristics in the area under investigation could be studied through a number of gradient maps (iso-parametric maps); that include, shale content ($V_{sh}$ %), effective porosity ($Ø_{eff}$ %) and hydrocarbon saturation ($S_{hr}$ %), to complete the vision of hydrocarbon potentialities in the studied area. The study of these parameters on maps is very important for judging about their lateral variations and the factors controlling them, which may be either structural, stratigraphic or both. (Figs. 27-32) illustrate combined petrophysical characteristics ($V_{sh}$, $Ø_{eff}$ and $S_{hr}$) for all studied layers.

### 1.1. Shale Content Distribution:

Shale content is a quantitative function of log analysis. It is considered as an important indicator of the reservoir quality, in which lower shale content usually reveals a better reservoir quality.

(Figure 27A) represents the shale content of Level-2. As shown in the figure, the shale content increases mainly to the eastern side and the far South West of the area under investigation. The clean sandstone is almost at the central part of the area under investigation around N-NW-2 and N-NW-3 wells. The maximum recorded value of shale content is 75% at East in N-9 well and decreasing gradually to the West at minimum 14% in N-NW-2.

(Figure 28A) represents the shale content of Level-3A. As shown in the figure, the shale content is generally low and increases little bit to the western side of the area under investigation. The clean sandstone is almost in everywhere in the channel. The maximum recorded value of shale content is 33% at West in N-6 well and decreasing gradually to the East and North at minimum 25% in N-10.

(Figure 29A) represents the shale content of Level-3. As shown in the figure, the shale content increases mainly to the western side of the area under investigation. The clean sandstone is almost in everywhere in the channel. The maximum recorded value of shale content is 20% at West in N-10 well and decreasing gradually to the East at minimum 5% in N-9 and N-11_ST3.

(Figure 30A) represents the shale content of Level-3 Lower. As shown in the figure, the shale content increases mainly to the eastern side of the area under investigation. The clean sandstone is almost in everywhere in the channel. The maximum recorded value of shale content is 13% at North East in N-9 well and decreasing gradually to the West and South.

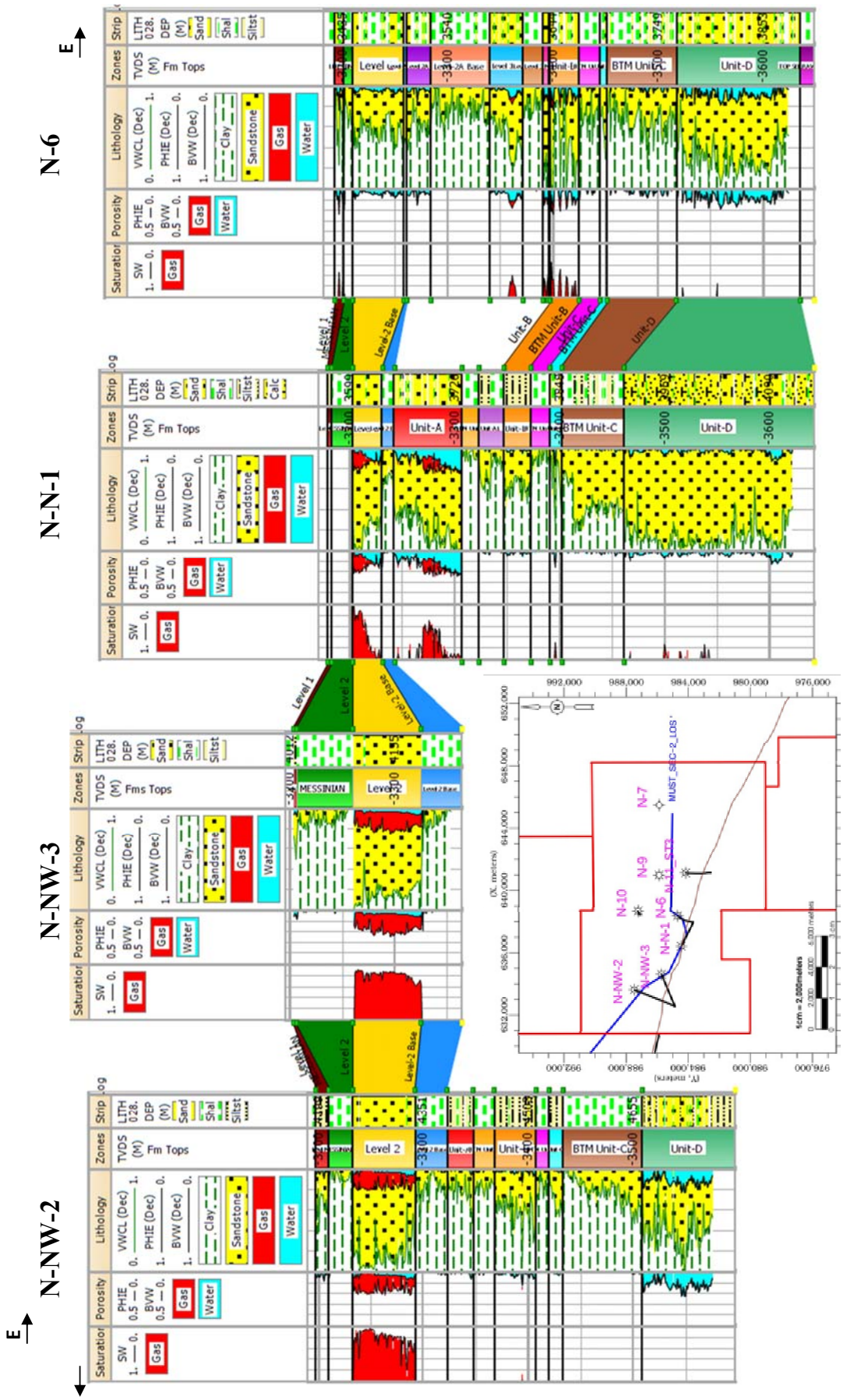


**Fig. 24: CPI Correlation Section (LOS-1), through N-NW-2, N-NW-3, N-N-1 and N-6 Wells.**

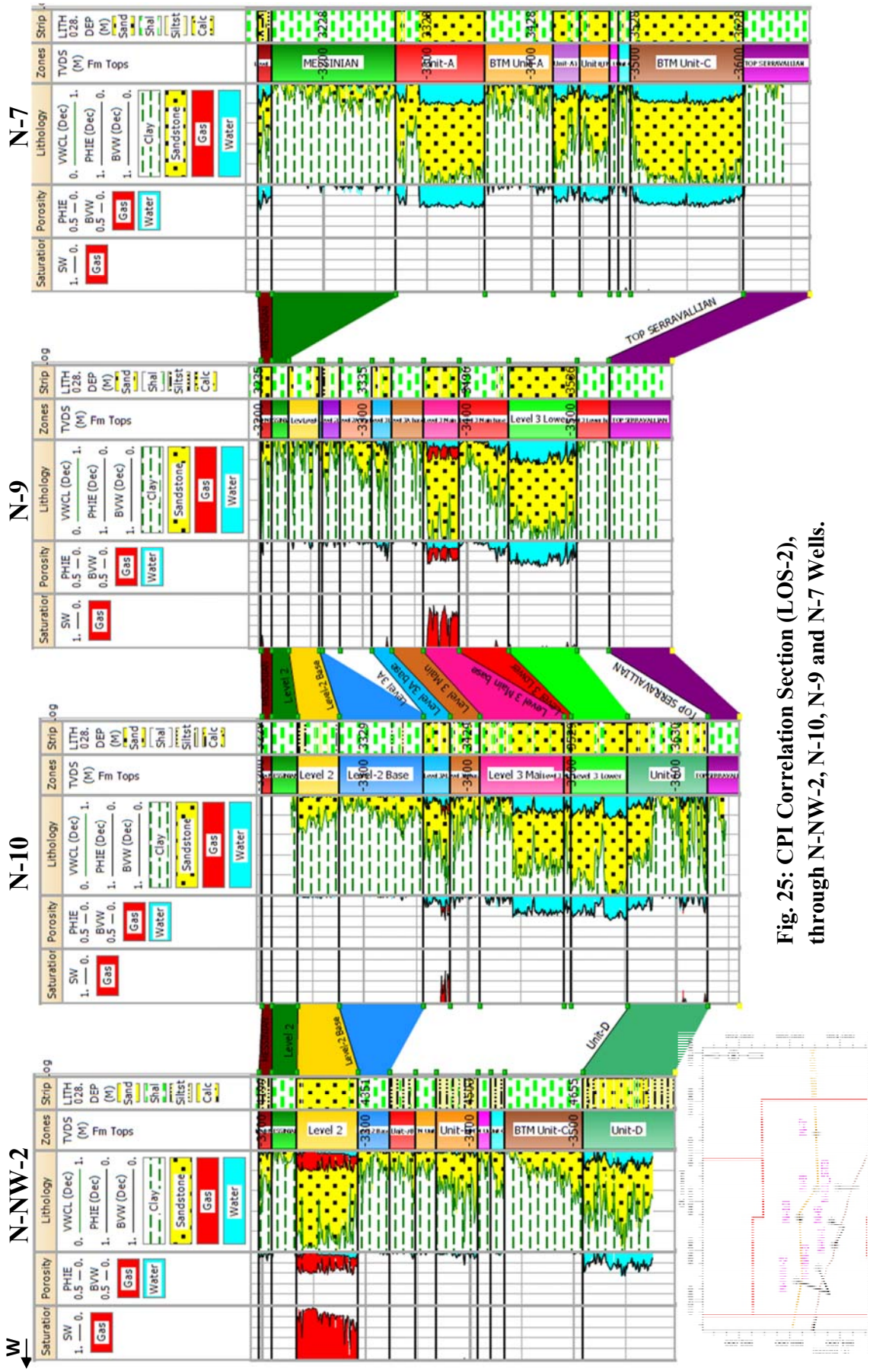


**Fig. 25: CPI Correlation Section (LOS-2), through N-NW-2, N-10, N-9 and N-7 Wells.**

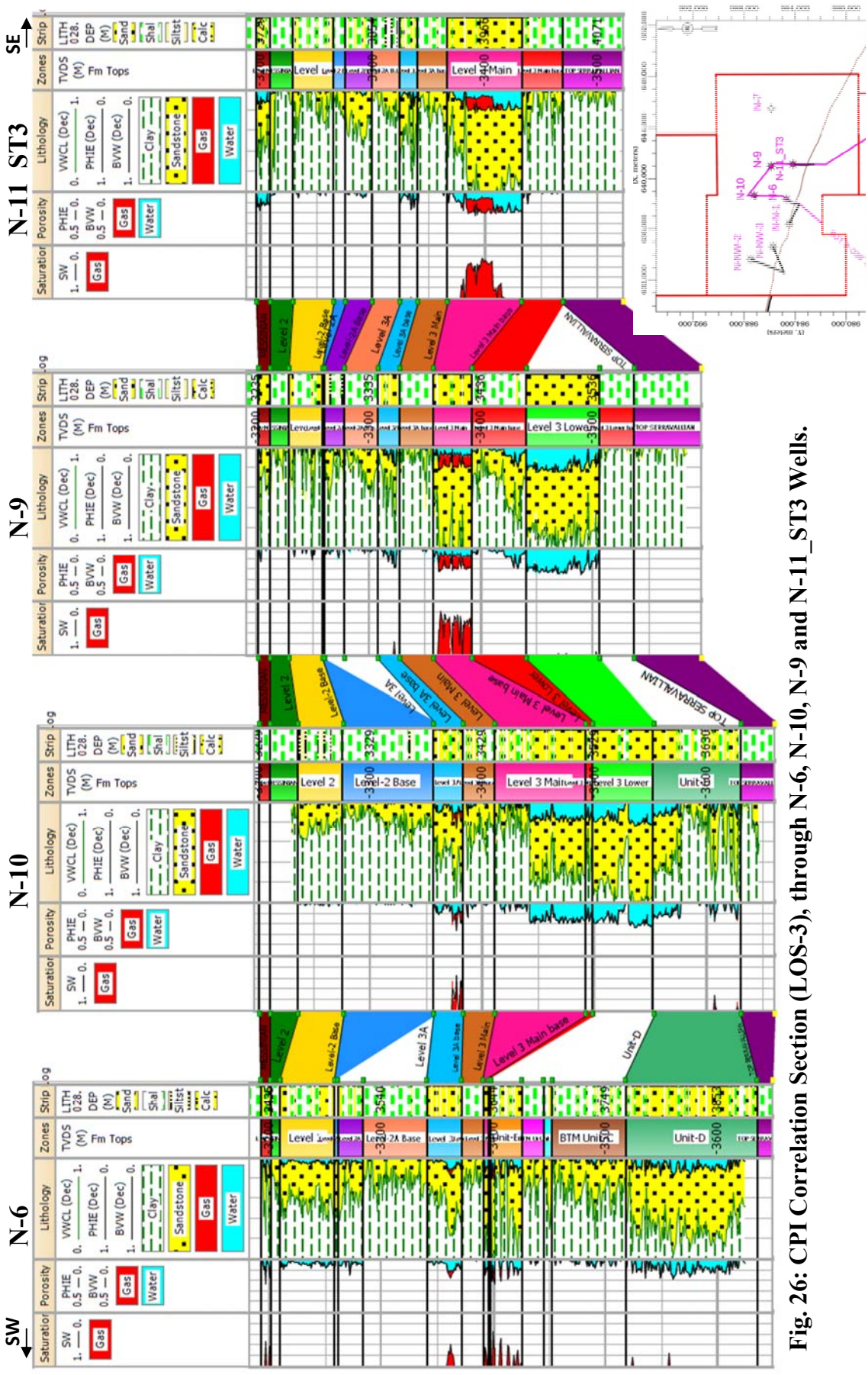


**Fig. 26: CPI Correlation Section (LOS-3), through N-6, N-10, N-9 and N-11_ST3 Wells.**

(Figure 31A) represents the shale content of Unit-A. As shown in the figure, the shale content increases mainly to the western side of the area under investigation. The clean sandstone is almost at the central and eastern part of the area under investigation. The maximum recorded value of shale content is 70% at West in N-NW-2 well and decreasing to the West at minimum 12% in N-7.

(Figure 32A) represents the shale content of Unit-B. As shown in the figure, the shale content increases mainly to the western side and the far East of the area under investigation. The clean sandstone is almost at the central part of the area under investigation around N-6 well. The maximum recorded value of shale content is 65% at the West in N-NW-2 well and decreasing gradually toward the center at minimum 9% in N-6 then start to increase again toward the East.

**1.2. Effective Porosity Distribution:**

Effective porosity is the most significant petrophysical character in the evaluation of hydrocarbon potentiality. The structural element may affect porosity development, which has a great influence on porosity (El Kadi et al., 2002).

(Figure 27B) represents the effective porosity distribution map of Level-2. As shown in the figure, it reflects that the effective porosity increases in the western part of the studied area within the center of the paleo-channel around N-NW-3 and N-NW-2 wells. The effective porosity recorded the maximum value of 19% in N-NW-3 well and the minimum value of 2% is recorded in N-10 well at the eastern border of the paleo-channel (central part of the studied area).

(Figure 28B) represents the effective porosity distribution map of Level-3A. As shown in the figure, it reflects that the effective porosity decreases in the western part of the studied area and the high effective porosity values are almost in everywhere in the channel. The effective porosity recorded the maximum value of 19% in N-10 well and the minimum value of 15% is recorded in N-6 well at the western border of the paleo-channel.

(Figure 29B) represents the effective porosity distribution map of Level-3. As shown in the figure, it reflects that the effective porosity decreases in the western part of the studied area and the high effective porosity values are almost in everywhere in the channel. The effective porosity recorded the maximum value of 20% in N-9 and N-11_ST3 wells and the minimum value of 14% is recorded in N-6 well at the western border of the paleo-channel.

(Figure 30B) represents the effective porosity distribution map of Level-3 Lower. As shown in the figure, it reflects that the effective porosity decreases little bit towards the eastern part of the studied area and the high effective porosity values are almost in everywhere in the channel. The effective porosity recorded the maximum value of 21% in N-10 and well and the minimum value of 20% is recorded in N-9 well.

(Figure 31B) represents the effective porosity distribution map of Unit-A. As shown in the figure, it reflects that the effective porosity increases in the eastern and central part of the studied area around N-7 and N-N-1 wells. The effective porosity recorded the maximum value of 21% in N-7 well and the minimum value of 4% is recorded in N-NW-2 well at the western part of the studied area.

(Figure 32B) represents the effective porosity distribution map of Unit-B. As shown in the figure, it reflects that the effective porosity increases in the eastern and central part of the studied area around N-7 and N-6 wells. The effective porosity recorded the maximum value of 18% in N-6 well and the minimum value of 4% is recorded in N-N-1 well at the southwestern part of the studied area.

**1.3. Hydrocarbon Saturation Distribution:**

Determination of hydrocarbon saturation is the main target in the current study. (Figure 27C) shows the hydrocarbon saturation map for Level-2. This figure reveals that the hydrocarbon saturation generally increases in the north western side of the studied area. The hydrocarbon saturation recorded the maximum value of 83% in N-NW-2 well and the minimum value of 0% is recorded in wells to the East and South.

(Figure 28C) shows the hydrocarbon saturation map for Level-3A. This figure reveals that the hydrocarbon saturation generally increases in the northern side of the studied area. The hydrocarbon saturation recorded the maximum value of 42% in N-10 well and the minimum value of 0% is recorded in N-11_ST3 well to the South.

(Figure 29C) shows the hydrocarbon saturation map for Level-3. This figure reveals that the hydrocarbon saturation generally increases in the central and southern part of the studied area. The hydrocarbon saturation recorded the maximum value of 72% in N-9 well and the minimum value of 0% is recorded in N-10 well to the North.

(Figure 30C) shows the hydrocarbon saturation map for Level-3 Lower. This figure reveals that the hydrocarbon saturation is generally low in this level and increases gradually in the southern part of the studied area. There is no hydrocarbon detected in the studied wells in this level. All drilled wells in this level are 100% water saturated.

(Figure 31C) shows the hydrocarbon saturation map for Unit-A. This figure reveals that the hydrocarbon saturation generally increases in the central and south eastern part of the studied area. The hydrocarbon saturation recorded the maximum value of 53% in N-N-1 well and the minimum value of 0% is recorded in N-NW-2 well to the West and N-7 to the East.

(Figure 32C) shows the hydrocarbon saturation map for Unit-B. This figure reveals that the hydrocarbon saturation generally increases in the central and north western part of the studied area. The hydrocarbon saturation recorded the maximum value of 56% in N-6 well and the minimum value of 0% is recorded in N-N-1 well to the southwest and N-7 to the East.

## SUMMARY AND CONCLUSIONS

Nidoco concession area is a large gas field located in the central part of the Nile Delta, along the coast of Mediterranean Sea. Nidoco Field is a multilayer one, with several separated sandstone reservoirs interbedded with shale intercalations. This paper deals mainly with a comprehensive interpretation of the available digital well-log data of eight wells scattered in the area of study, to delineate the hydrocarbon potentialities of the Late Miocene section.

The well-log analysis was started by cross plots evaluation. Tri-porosity (M-N) cross-plots for mineral identifications were used, to detect in general the types of lithology. The tri-porosity (M-N) cross-plots showed that, the main minerals are quartz, shales and few calcites. Lithologic identification was achieved through cross-plots between $\rho_b$, $Ø_n$ and $\Delta t$ to detect the exact lithology for each layer. These charts showed that, sandstone and shale represent the main components of the Late Miocene section. Pickett's plots were constructed to determine the formation water resistivity ($R_w$), and water and hydrocarbon saturations ($S_w$ and $S_{hr}$). The resulted formation water resistivity ranges from 0.138 Ohm.m to 0.20 Ohm.m, and the obtained hydrocarbon saturations range from 83% to 0%. Dia-porosity cross-plots were established, to determine the shale volume and effective porosity. The obtained shale volume ranges from 3% to 45% and the produced effective porosity ranges from 8% to 20 %. Shale types cross-plots were used also, to detect the shale types in the studied section, which are mainly laminated with some mixture of dispersed and laminated shales. Shale minerals cross-plots were used too and indicated that, Montmorillonite is the main mineral component of shale in the studied section

.

All petrophysical characteristics of the studied wells were represented vertically in the form of litho-saturation cross-plots, as inferred from computer processed interpretation (CPI). The lateral variations of the mentioned petrophysical characteristics were represented in the form of iso-parametric maps ((shale content ($V_{sh}$), effective porosity ($Ø_{eff}$) and hydrocarbon saturation ($S_{hr}$)).

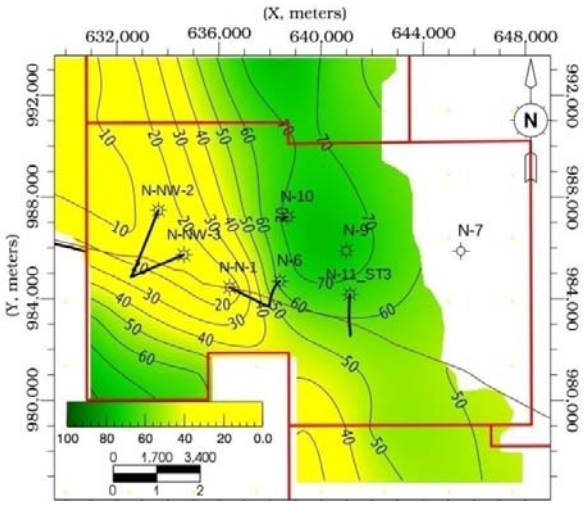


(A) Shale Content (%) **C.I. = 10**

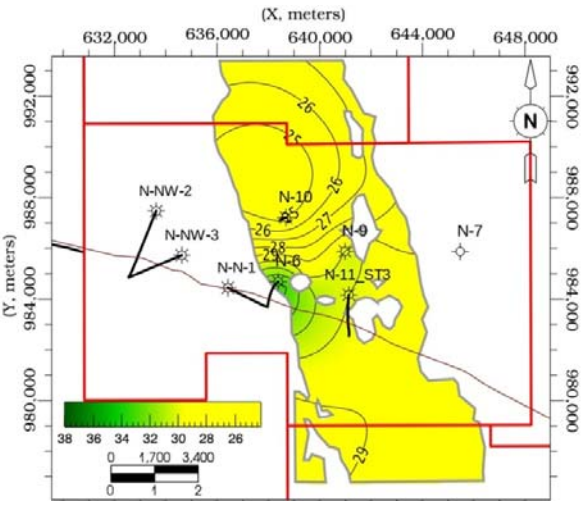


(A) Shale Content (%) **C.I. = 1**

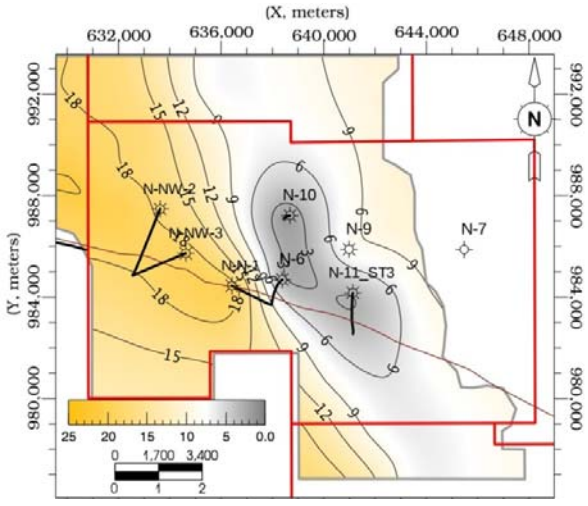


(B) Effective Porosity (%) **C.I. = 3**

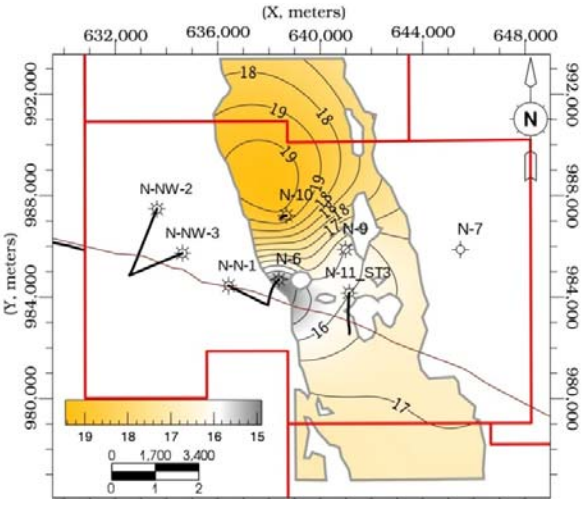


(B) Effective Porosity (%) **C.I. = 1**

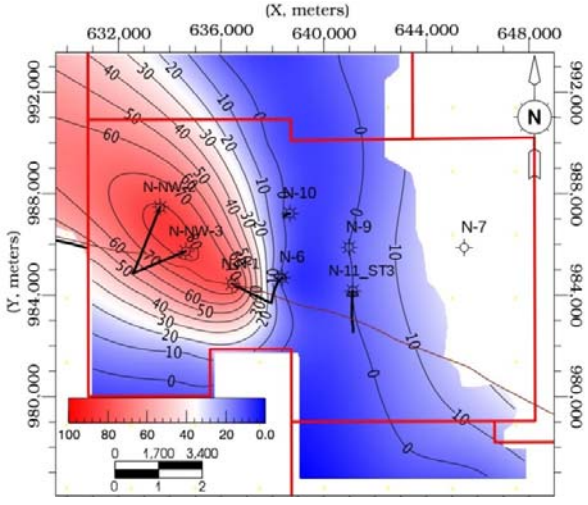


(C) Hydrocarbon Saturation (%) **C.I. = 10**

**Fig. 27: Combined Petrophysical Distribution Parameters of Level-2.**

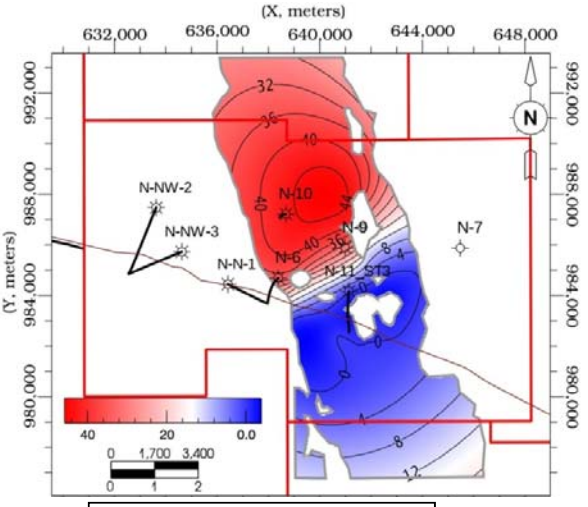


(C) Hydrocarbon Saturation (%) **C.I. = 4**

**Fig. 28: Combined Petrophysical Distribution Parameters of Level-3A.**

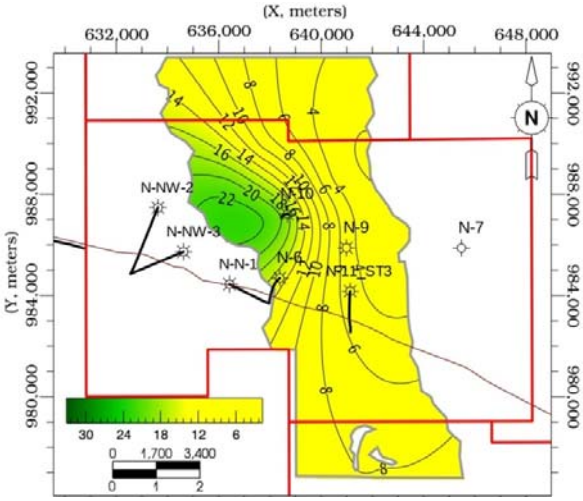


(A) Shale Content (%) C.I. = 2

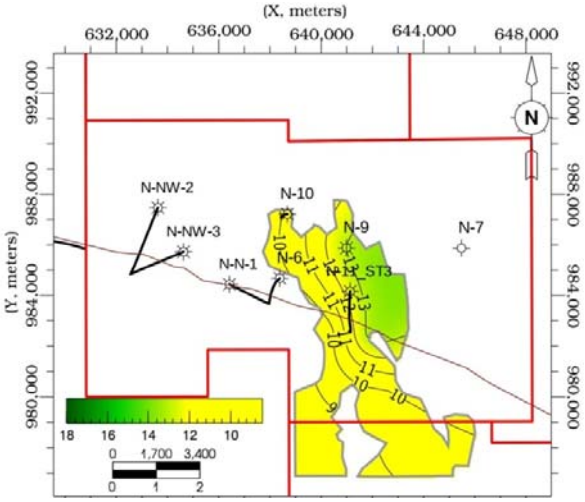


(A) Shale Content (%) C.I. = 1

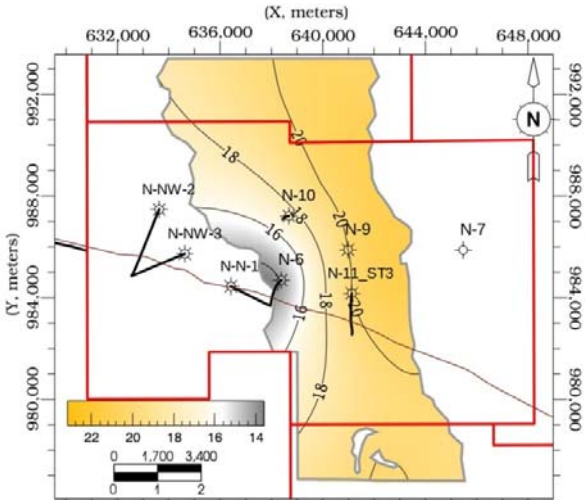


(B) Effective Porosity (%) C.I. = 2

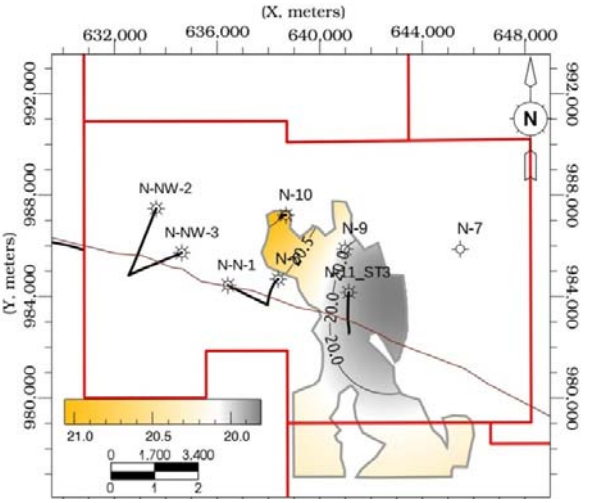


(B) Effective Porosity (%) C.I. = 0.5

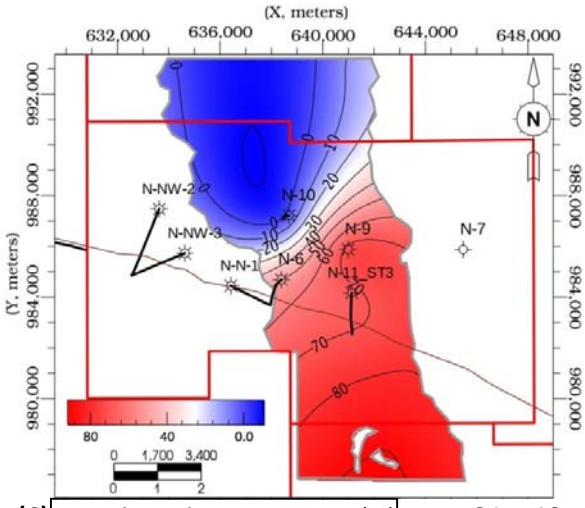


(C) Hydrocarbon Saturation (%) C.I. = 10

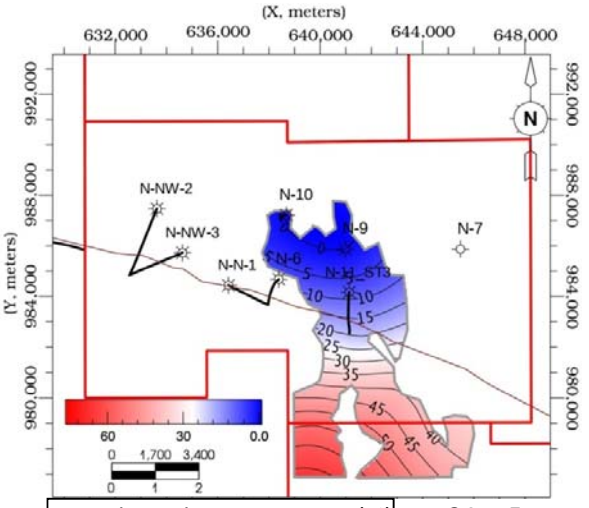


(C) Hydrocarbon Saturation (%) C.I. = 5

**Fig. 29: Combined Petrophysical Distribution Parameters of Level-3.**

**Fig. 30: Combined Petrophysical Distribution Parameters of Level-3 Lower.**

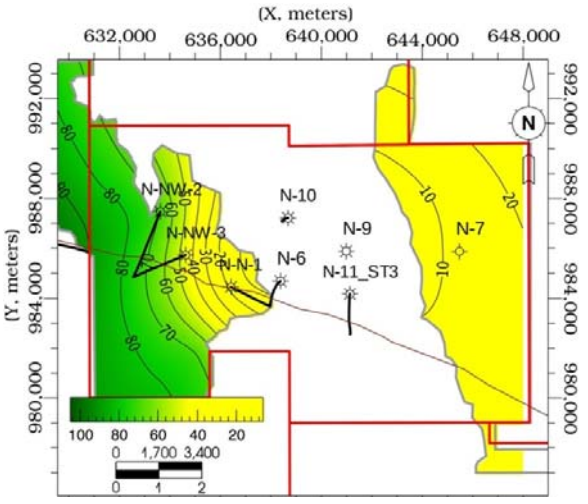


(A) Shale Content (%) C.I. = 10

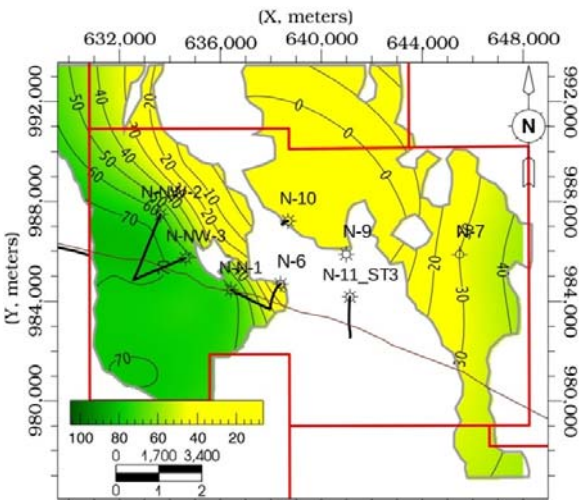


(A) Shale Content (%) C.I. = 10

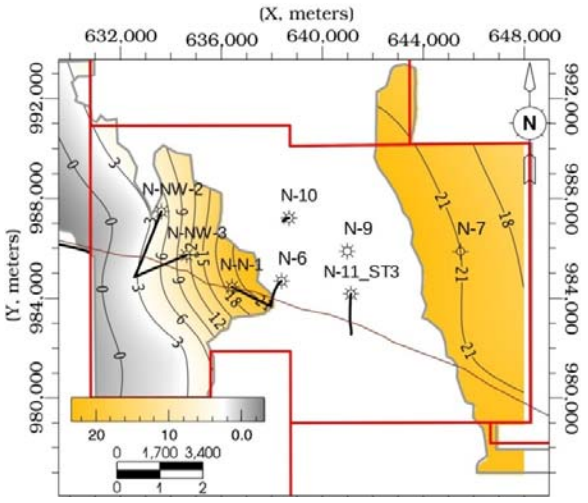


(B) Effective Porosity (%) C.I. = 3

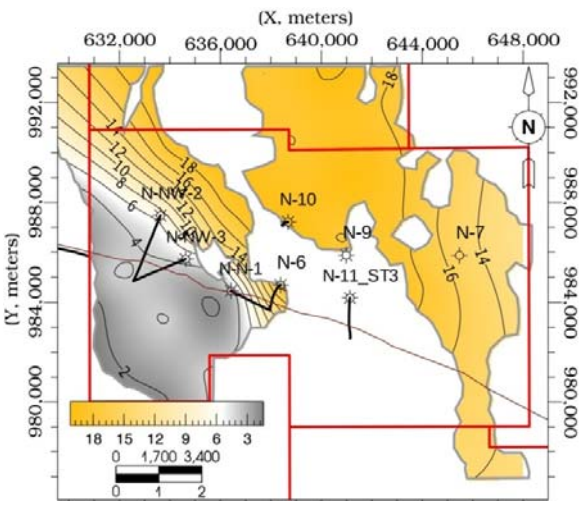


(B) Effective Porosity (%) C.I. = 2

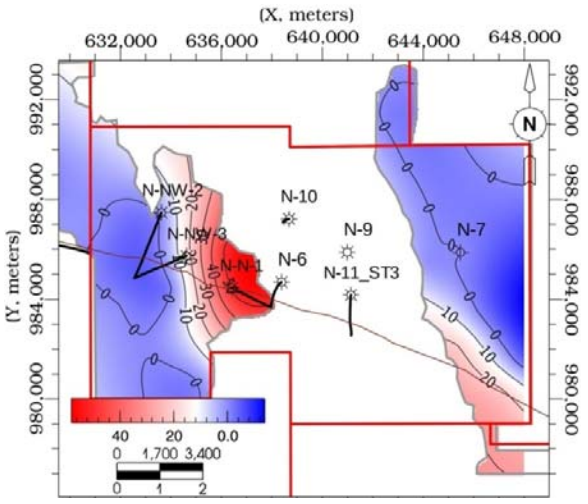


(C) Hydrocarbon Saturation (%) C.I. = 10

**Fig. 31: Combined Petrophysical Distribution Parameters of Unit-A.**

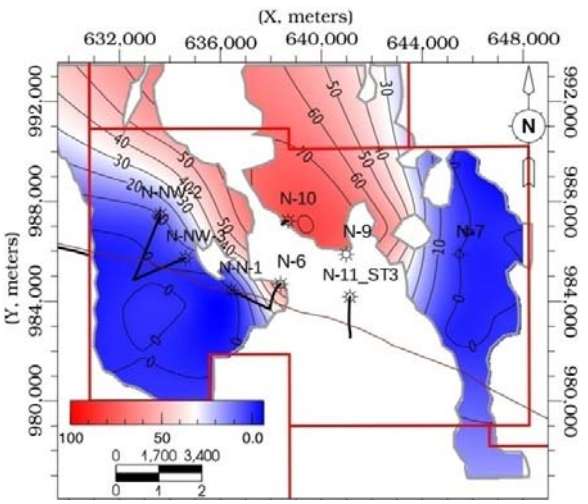


(C) Hydrocarbon Saturation (%) C.I. = 10

**Fig. 32: Combined Petrophysical Distribution Parameters of Unit-B.**

From the previously mentioned petrophysical characteristics of the studied levels and units, it is obvious that, some layers have the ability to store and produce hydrocarbon more than others. It is clear that, Level-2, Level-3A, Level-3, Level-3 Lower, Unit-A and Unit-B are showing better reservoir characterization and higher gas potentialities than the rest of the studied levels and units. The integration of all the mentioned available well data has allowed huge gas discoveries to be achieved.

It is recommended to drill more exploratory and development wells to produce more hydrocarbons, especially from Level-2 toward the northwestern part of the study area, Level-3A toward the southern part, Level-3 toward the northwestern, southern and eastern parts, Level-3 Lower toward the southern part, Unit-A toward the northwestern and southern parts, and Unit-B toward the northwestern and northern parts of the study area, which still showing high hydrocarbon potentialities.

## REFERENCES

Burke J. A., Campbell R. L. and Schmidt A. W., 1969, "The Litho porosity Cross-plots", SPWLA, 10th Ann. Symp. Trans., pp. 1-29.

Darwin. V. Ells, 1987, "Well Logging for Earth Scientists", Elsevier Science Publishing Co., Inc. New York, pp. 401-447.

El-Kadi H. H., E. A. Abd EI-Gawad and A. M. Ghazaly, 2002, "Reservoir Characterization of the Upper Cretaceous Formations at Dabaa- Al Amein Area, North Western Desert, Egypt", J. Appl. Geophs., Vol. 1, September 2002, pp. 33-52.

Eni/Agip Internal Study, 2000, "Egypt – Offshore Nile Delta: Integrated Regional Study", Milan, Italy.

Mody G.B., 1961, "Petroleum Exploration Handbook", Mc Graw Hill Book Company, New York. Chapter 19 (Electrical Logging) by H.G. Doll, p. 1-19 to 19-41.

Pirson, 1977, "Geologic Well Log Analysis", Gulf Publishing Company. Huston, London, Paris. pp. 165-169.

Schlumberger, 1972, Log Interpretation Vol. I Principles. Schlumberger Limited, New York, U.S.A, p. 112.